Applying Image Restoration to Fluorescence Lifetime Imaging Microscopy (FLIM)

Ching-Wei Chang[1] and Mary-Ann Mycek[1, 2, 3]

[1]*Department of Biomedical Engineering, University of Michigan, Ann Arbor, MI 48109-2099*
[2]*Comprehensive Cancer Center, University of Michigan, Ann Arbor, MI 48109-2099*
[3]*Applied Physics Program, University of Michigan, Ann Arbor, MI 48109-2099*
mycek@umich.edu

Abstract: We describe a novel approach using 2D-intensity-deconvolution to improve spatial resolution in wide-field FLIM. The method maintains lifetime accuracy and can restore features within experimentally reasonable intensity ranges.

©2009 Optical Society of America
OCIS codes: (100.2000) Digital image processing; (170.6920) Time-resolved imaging.

1. Introduction

Fluorescence lifetime imaging microscopy (FLIM) is a method to retrieve lifetime data from fluorescence emission after excitation. FLIM has some advantages over intensity-based measurements since it is insensitive to artifacts influencing fluorescence intensity, such as optical loss, photobleaching, and differences in fluorophore concentration [1-3].

It is commonly known that the imaging properties of any optical microscope give rise to spatial distortions [4]. While theoretically insensitive to intensity, lifetime images are derived via intensity image analysis in several FLIM techniques [5]. As a result, poor quality lifetime maps may be partially the result of distorted intensity images.

With advances in desktop computing power, numerical methods are providing an increasingly efficient way to improve resolution without compromising signal-to-noise ratio (SNR) or the need for additional optical hardware. Recently, we demonstrated that a commercial version of an iterative constrained 2D blind image restoration algorithm can be applied successfully to FLIM intensity images [6].

Here, we present the resolution enhancement of FLIM lifetime maps and further investigate the lifetime changes after image restoration when one single image contains samples with different signal intensities (or SNR).

2. Methods

2.1. Fluorescence Lifetime Imaging Microscopy (FLIM)

To implement time-gated FLIM, recently we have designed and characterized a novel time-domain, wide-field FLIM system for picosecond time-resolved imaging for biological applications [7]. A dye laser pumped by a nitrogen laser for UV-visible-NIR excitation provides a wide-field, less expensive, and potentially portable alternative to multi-photon excitation for sub-nanosecond FLIM of biological specimens [7]. A sample is illuminated by an excitation pulse and the fluorescence emission is recorded by an intensified charge-coupled device (ICCD) camera at a gate delay controlled by the intensifier, with emission intensities integrated during a gate width. This system has a large temporal dynamic range (750 ps – 1 μs), 50 ps lifetime discrimination, and spatial resolution of 1.4 μm, which make it very suitable for studying a variety of endogenous and exogenous fluorophores in

Advanced Microscopy Techniques, edited by Paul J. Campagnola, Ernst H. K. Stelzer, Gert von Bally, Proc. of SPIE-OSA Biomedical Optics, SPIE Vol. 7367, 73671E · © 2009 SPIE-OSA · CCC code: 1605-7422/09/$18 · doi: 10.1117/12.831498

biological samples [2, 8, 9]. Fluorescence lifetime maps are determined by first acquiring fluorescence intensity images at four gate delays and then calculating the lifetime values from the intensity decay on a pixel-by-pixel basis (further described below).

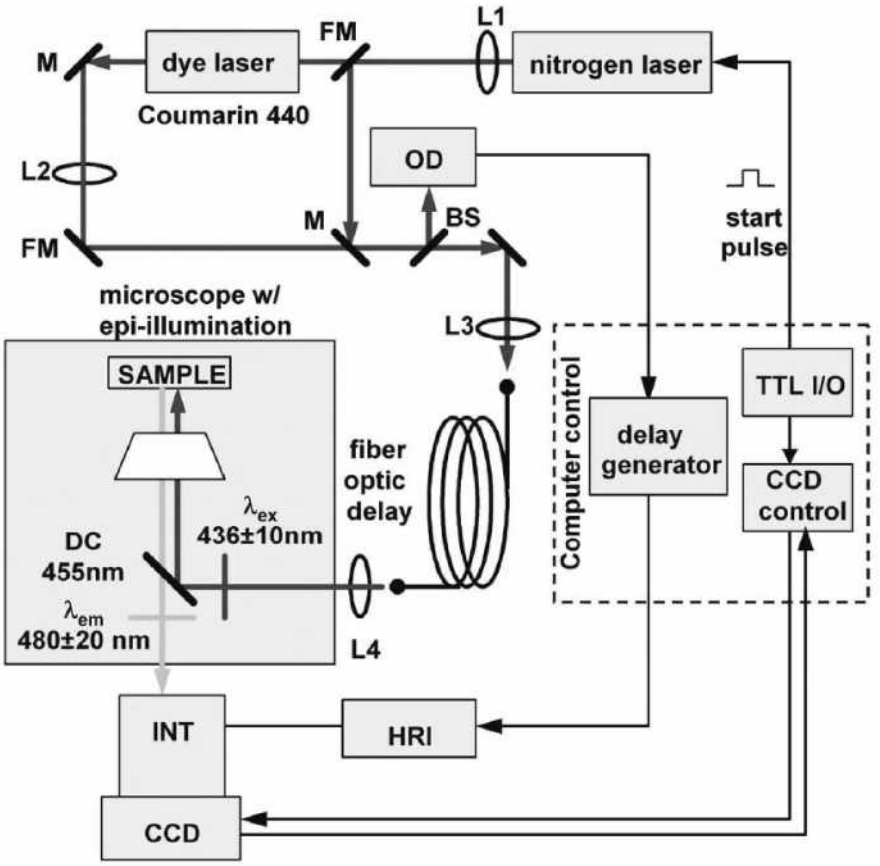

Figure 1 The time-gated FLIM setup used for this study. Abbreviations: CCD = charge-coupled device; HRI = high rate imager; INT = intensifier; TTL I/O = TTL input/output card; OD = optical discriminator; BS = beam splitter; DC = dichroic mirror; FM = "flippable" mirror; L1, L2, L3, L4 = quartz lenses; M = mirror. Thick solid lines = light path; thin solid line = electronic path. [10]

Figure 1 illustrates our FLIM system instrumentation, with some main experimental specifications for imaging living cells described below. The excitation source was composed of a pulsed nitrogen laser (GL-3300, Photon Technology International, Lawrenceville, NJ) pumping a dye laser (GL-301, Photon Technology International, Lawrenceville, NJ), with a wavelength range from UV through near infrared (NIR), depending on the dye in use. An optical fiber (SFS600/660N, Fiberguide Industries, Stirling, NJ) was used to deliver the excitation light to a research-grade, inverted microscope (Axiovert S100 2TV, Zeiss, Germany) in epi-illumination mode. The optical fiber had the added benefit of homogenizing the spatial intensity distribution of the beam. A beam splitter split a reference pulse from the excitation light and sent it to an optical discriminator to generate an electronic pulse, which offered a time reference to a picosecond delay generator (DEL350, Becker & Hickl, Germany), whose output was then used for triggering the gated intensified CCD (ICCD) camera (Picostar HR, LaVision, Germany). The ICCD

had variable intensifier gain and gate width settings varying from 200 ps to 10 ms and can be used to implement high-speed imaging in other applications as well [11].

2.2. Image Restoration

The image restoration procedure has been described previously [6]. The restoration of each gated intensity image was implemented by using the Autoquant® (Media Cybernetics, Bethesda, MD) software. The underlying Maximum Likelihood Estimation (MLE) algorithm, a mathematical optimization approach generally used to provide estimates of quantities corrupted by some kind of random noise, serves as the basis of the 2D Blind approach and has been explained elsewhere [12, 13]. Briely, image restoration and/or deconvolution are performed in a set of processes for reversing the optical distortion that occurs in a microscope. It is often assumed that the original uncorrupted image is distorted by an instrument response, which can be defined by the point spread function (PSF) of the imaging system in use. The PSF is the image of an infinitely small point source, and can be estimated by either a) imaging a sample (for example, a fluorescent bead) of smaller size than the resolution of the microscope, or b) estimating theoretically the PSF by the parameters of the imaging system, in particular, the objective lens. The latter method is what is known as the blind method. Blind image restoration method, therefore, attempts to recover the original uncorrupted image by deconvolving the estimated PSF from the given observed image.

After image acquisition, Autoquant® was then used to blindly 2D-deconvolve the first of the four time gates used to obtain the lifetime map with the FLIM system. From the deconvolution of the first image, a derived point spread function was obtained, which was then used in the 2D deconvolution (i.e., non-blind) of the three remaining gates. The number of iterations was set to 10 unless otherwise noted. The computationally-restored images were then analyzed for lifetime.

2.3. Lifetime Determination

To creating fluorescence lifetime maps rapidly, a four-gate protocol with a linearized least squares lifetime determination method is used on a pixel-by-pixel basis [5, 14, 15]:

$$\tau_p = -\frac{N(\sum t_i^2) - (\sum t_i)^2}{N\sum t_i \ln I_{i,p} - (\sum t_i)(\sum \ln I_{i,p})}$$

where τ_p is the lifetime of pixel p, $I_{i,p}$ is the intensity of pixel p in image i, t_i is the gate delay of image i, and N is the number of images. All sums are over i.

Additional steps in data processing are needed for more accurate lifetime map production. Before lifetime calculation, the step “background subtraction” takes average of the intensities of pixels within a specified background region and subtracts that average value from all pixels. Also, the step “reject” sets intensities to zero for all pixels with intensities below a certain value (assigned as the parameter “reject”) after background subtraction. After lifetime calculation, the step “tau range” sets lifetime to zero for all pixels with lifetime above a certain value (assigned as the parameter “taurange”) after lifetime calculation, to remove lifetime values in physically meaningless regions. In this study, “reject” was set to 15 and “taurange” was set to 30.

2.4. Sample Preparation

10 μm fluorescent beads (Polysciences, Warrington, PA) were suspended in distilled water to produce solutions with concentrations of $3x10^6$ beads/mL. Before imaging, 200 μL of each solution was placed on a delta T dish (Bioptechs, Butler, PA), and imaging was begun after the beads had settled to the bottom of the dish. All beads had excitation/emission maxima of 441/486 nm, as specified by the manufacturer. A 100 x objective was used in the FLIM microscope.

2.5. Data Analysis

On the lifetime map constructed from the restored intensity images, a selection was made of eight regions that exhibited different intensities. In each of these regions, the average intensity and lifetime values (over all nonzero pixels) were calculated. Then, the percentage change in mean lifetime (%τ), relative to the native image, was calculated for each region and plotted against the intensity (I) in that region. The following notations were used: N(I): native intensity image; N(τ): native lifetime map; R(I): restored intensity image; R(τ): restored lifetime map.

3. Results

3.1. FLIM Image Restoration

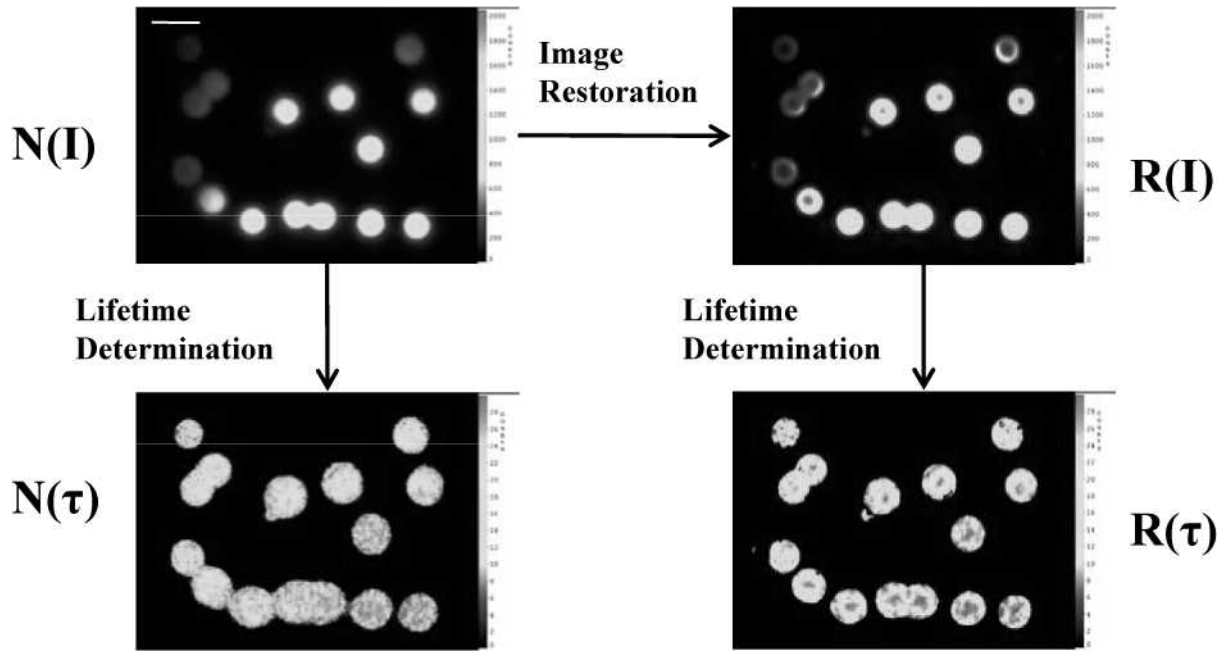

Figure 2 Relationships between N(I): native intensity image, N(τ): native lifetime map, R(I): restored intensity image, and R(τ): restored lifetime map. By applying image restoration to FLIM, the irresolvable features in N(τ), such as the beads in the lower-left portion, became resolved in R(τ). Scale bar: 20 μm.

Figure 2 demonstrates our FLIM image restoration procedures. The lifetime determination algorithm can be applied directly to the native intensity images, N(I), to produce the native lifetime map, N(τ). In this case, some beads that were resolved in N(I) could not be resolved in N(τ), such as the beads in the lower-left portion of the image. Image restoration was then applied to N(I), and R(I) was produced. The lifetime determination algorithm then could be

applied to R(I) to produced R(τ), and the previously irresolvable features in N(τ) (the beads in the lower-left portion) became resolved in R(τ). In addition, compared to the beads in N(τ), the beads in R(τ) had smaller diameters (~12 – 13 μm), which were actually closer to the real diameters of the beads as shown in N(I) and R(I) (~12 μm). On the other hand, the beads in N(τ) had diameters of ~18 μm.

3.2. Restoring Features with Different SNR Values

Figure 3 shows that for very low signal intensities, the measured percentage changes in lifetime tended to decrease with increasing SNR. The eight points were obtained from the intensity images and lifetime maps shown in Fig. 1. At the lowest recorded intensities (50 counts) the lifetime change was just under 15%. The results also indicated that once the intensity reached 200 counts, the percentage lifetime change fell below 5%. With this trend, we expect the percentage changes to approach zero as the intensity further increases. A reasonable range of intensities is greater than or equal to 150 counts (or even 200 counts) in our typical FLIM measurements, and FLIM image restoration in this range provides a percentage change in lifetime lower than 10% (or 5%).

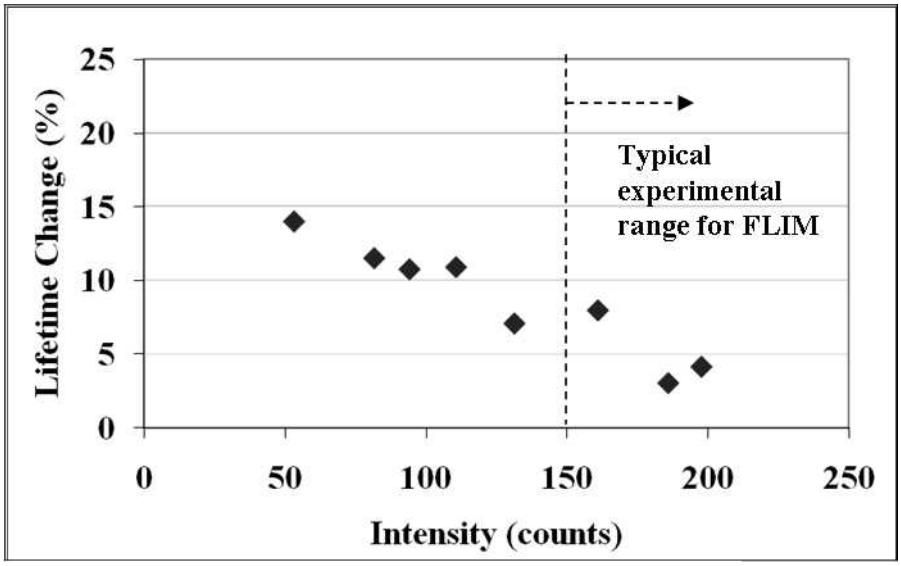

Figure 3 Percentage lifetime change (relative to native lifetime map) plotted against intensity for eight separate regions of the restored lifetime map, corresponding to eight beads with different SNR values. The percentage changes in lifetime tend to decrease with increasing SNR and fall below 10% when intensity is greater than 150 counts, which is a typical intensity range for our experiments.

4. Discussion and Future Work

The denoising process in the image restoration algorithm may explain the trend that the percentage change in lifetime decreases with increasing SNR. With the shot noise (or quantum noise) in our CCD camera, since the images at later gates had weaker signals, they had, according to Poisson noise distribution, relatively higher noise level compared to the images at earlier gates. In addition, the images at later gates tended to be corrupted to relatively more extent by the readout noise, which had a constant magnitude due to the fixed readout rate of our CCD camera at 12.5 MHz. In this study, the noise setting was fixed at "medium" at all four gates for consistency in the image restoration algorithm. This, therefore, could result in insufficient denoising at later gates, thereby producing higher intensity than at earlier gates, and hence, higher lifetime. Since this effect is more pronounced for lower-intensity features in the image, it may explain why lower SNR correlates with a greater change in lifetime

after image restoration. Future studies will include setting the noise level higher for later gates, where SNR values are smaller. Additional work will investigate limitations to this image restoration approach for FLIM samples with varying feature sizes and multiple fluorophore lifetimes.

In summary, we presented a novel approach using 2D-intensity-deconvolution to improve spatial resolution in wide-field FLIM maps. The method maintains lifetime accuracy to better than 10% and can restore features within experimentally reasonable intensity ranges.

5. References

1. Chen, Y., J.D. Mills, and A. Periasamy, *Protein localization in living cells and tissues using FRET and FLIM.* Differentiation, 2003. **71**(9-10): p. 528-541.
2. Urayama, P.K. and M.A. Mycek, *Fluorescence lifetime imaging microscopy of endogenous biological fluorescence*, in *Handbook of Biomedical Fluorescence*, M.A. Mycek and B.W. Pogue, Editors. 2003, Marcel Dekker, Inc.: New York.
3. Chang, C.W., D. Sud, and M.A. Mycek, *Fluorescence lifetime imaging microscopy.* Methods Cell Biol, 2007. **81**: p. 495-524.
4. Goodwin, P.C., *Evaluating optical aberration using fluorescent microspheres: methods, analysis, and corrective actions.* Methods Cell Biol, 2007. **81**: p. 397-413.
5. Sharman, K.K., A. Periasamy, H. Ashworth, J.N. Demas, and N.H. Snow, *Error analysis of the rapid lifetime determination method for double-exponential decays and new windowing schemes.* Analytical Chemistry, 1999. **71**(5): p. 947-952.
6. Sud, D. and M.A. Mycek, *Image restoration for fluorescence lifetime imaging microscopy (FLIM).* Optics Express, 2008. **16**(23): p. 19192-19200.
7. Urayama, P., W. Zhong, J.A. Beamish, F.K. Minn, R.D. Sloboda, K.H. Dragnev, E. Dmitrovsky, and M.A. Mycek, *A UV-visible-NIR fluorescence lifetime imaging microscope for laser-based biological sensing with picosecond resolution.* Applied Physics B-Lasers and Optics, 2003. **76**(5): p. 483-496.
8. Urayama, P.K., J.A. Beamish, F.K. Minn, E.A. Hamon, and M.-A. Mycek. *A UV fluorescence lifetime imaging microscope to probe endogenous cellular fluorescence*. in *Conference on Lasers and Electro-Optics*. 2002: Optical Society of America, Washington D.C.
9. Zhong, W., P. Urayama, and M.-A. Mycek, *Imaging fluorescence lifetime modulation of a ruthenium-based dye in living cells: the potential for oxygen sensing.* Journal of Physics D: Applied Physics, 2003. **36**(14): p. 1689-1695.
10. Zhong, W., M. Wu, C.W. Chang, K.A. Merrick, S.D. Merajver, and M.A. Mycek, *Picosecond-resolution fluorescence lifetime imaging microscopy: a useful tool for sensing molecular interactions in vivo via FRET.* Optics Express, 2007. **15**(26): p. 18220-18235.
11. Xu, Z., M. Raghavan, T.L. Hall, C.W. Chang, M.A. Mycek, J.B. Fowlkes, and C.A. Cain, *High speed imaging of bubble clouds generated in pulsed ultrasound cavitational therapy-histotripsy.* Ieee Transactions on Ultrasonics Ferroelectrics and Frequency Control, 2007. **54**(10): p. 2091-2101.
12. Markham, J. and J.A. Conchello, *Fast maximum-likelihood image-restoration algorithms for three-dimensional fluorescence microscopy.* Journal of the Optical Society of America a-Optics Image Science and Vision, 2001. **18**(5): p. 1062-1071.
13. Verveer, P.J., M.J. Gemkow, and T.M. Jovin, *A comparison of image restoration approaches applied to three-dimensional confocal and wide-field fluorescence microscopy.* Journal of Microscopy-Oxford, 1999. **193**: p. 50-61.
14. Bugiel, I., K. König, and H. Wabnitz, *Investigation of cell by fluorescence laser scanning microscopy with subnanosecond time resolution.* Lasers in the Life Sciences, 1989. **3**(1): p. 47-53.
15. Wang, X.F., T. Uchida, D.M. Coleman, and S. Minami, *A two-dimensional fluorescence lifetime imaging system using a gated image intensifier.* Applied Spectroscopy, 1991. **45**(3): p. 360-366.